Electronic structure and weak itinerant magnetism in metallic Y_2Ni_7

David J. Singh*

Department of Physics and Astronomy, University of Missouri, Columbia, Missouri 65211-7010, USA

(Received 15 May 2015; revised manuscript received 13 October 2015; published 3 November 2015)

We report a density functional study of the electronic structure and magnetism of Y_2Ni_7. The results show itinerant magnetism very similar to that in the weak itinerant ferromagnet Ni_3Al. The electropositive Y atoms in Y_2Ni_7 donate charge to the Ni host mostly in the form of s electrons. The non-spin-polarized state shows a high density of states at the Fermi level, $N(E_F)$, due to flat bands. This leads to a ferromagnetic instability. However, there are also several much more dispersive bands crossing $E(F)$, which should promote the conductivity. Spin fluctuation effects appear to be comparable to or weaker than Ni_3Al, based on comparison with experimental data. Y_2Ni_7 provides a uniaxial analog to cubic Ni_3Al for studying weak itinerant ferromagnetism, suggesting detailed measurements of its low temperature physical properties and spin fluctuations, as well as experiments under pressure.

DOI: 10.1103/PhysRevB.92.174403 PACS number(s): 75.10.Lp, 75.50.Cc, 71.20.Be

I. INTRODUCTION

Weak itinerant ferromagnetism is a topic of ongoing interest, both from the point of view of understanding the physical behavior of metals near quantum critical points, and because of the fact that these materials often have relatively high ordering temperatures when scaled to the ordered moment. There is also renewed interest in itinerant magnetism because of the unusual magnetic properties of the Fe-based superconductors [1–4] and spin-fluctuation pairing models for these and other unconventional superconductors [5–11].

Elemental fcc Ni metal is a classic example of an itinerant ferromagnet. Substitution by 25% with the trivalent element Al to form Ni_3Al strongly reduces the Curie temperature to yield a weak itinerant ferromagnet near a critical point that can be reached under pressure [12,13]. Both Ni_3Al and Ni_3Ga show evidence for strong exchange enhancement and spin-fluctuation effects, including quantum spin fluctuation induced suppression of ferromagnetism [14,15] in Ni_3Ga [13,16–22]. These two compounds have very similar electronic structures, and differ mainly in the strength of the quantum spin fluctuations. This difference places them on opposite sides of a ferromagnetic quantum critical point at ambient pressure. Unusual physical behavior including non-Fermi liquid scalings extending to very low temperature has been found in Ni_3Al under pressure [13].

Y_2Ni_7 forms in a rhombohedral ($R\bar{3}m$) Gd_2Co_7 structure [23–25] and is a ferromagnet [26–30]. The magnetism is unusual in that it has a high Curie temperature of $T_C \sim 54$ K relative to the moment size, reported as $m = 0.06\ \mu_B$–$0.08\ \mu_B$ per Ni [26,27]. If one scales the Curie temperature of elemental Ni ($T_C = 627$ K), which is also high relative to its moment size, by the square of the moment as usual, one would infer an expected Curie temperature of only ∼6–7 K for Y_2Ni_7. The system is also unusual in that, in spite of the high T_C, it is very sensitive to alloying, both by H incorporation [26] and by metal alloying [31,32]. Here, we investigate the magnetic and electronic properties of Y_2Ni_7 in relation to Ni metal as well as the weak itinerant ferromagnet Ni_3Al and the related compound Ni_3Ga. We find a behavior reminiscent of Ni_3Al.

II. METHODS AND STRUCTURE

The present density functional calculations were done using the generalized gradient approximation of Perdew, Burke, and Ernzerhof [33] and the linearized augmented plane-wave (LAPW) method [34] as implemented in the WIEN2K code [35]. We also performed calculations using the local spin density approximation (LSDA) and we also tested the effects of spin-orbit coupling. We used well converged basis sets, with a plane-wave cutoff, K_{max} determined by $R_{min}K_{max} = 9$, where R_{min} is the smallest sphere radius, here 2.25 Bohr for both Y and Ni. The calculations were done using the experimental lattice parameters [25]: $a = 4.947$ Å and $c = 36.25$ Å. The internal coordinates were determined by total energy minimization. For this purpose we started with the structure of the prototype (Gd_2Co_7). The resulting structure is given in Table I and depicted in Fig. 1. Plasma frequencies were determined using the optical package of the WIEN2K code, which uses integration of the squared band velocity on the Fermi surface for this purpose. In this code, the velocities come from calculations of the dipole (momentum) operator.

III. RESULTS AND DISCUSSION

Y_2Ni_7, which is ∼78% Ni, has metal atoms in distorted 12-fold cages. As mentioned, Ni_3Al, which contains 75% Ni, also with a trivalent element has suppressed ferromagnetism relative to Ni and is near an interesting quantum critical point [13,19,22]. Ni_3Al has $T_C = 41.5$ K, $M = 0.08\ \mu_B$/Ni, similar to Y_2Ni_7. One signature of the physical importance of fluctuations associated with the quantum critical point in Ni_3Al is an overestimate of the ordered moment in standard density functional calculations. In the case of Ni_3Al, the calculated spin moment in the local density approximation is $M_{LDA} = 0.24\ \mu_B$/Ni [21].

For Y_2Ni_7, we obtain a spin magnetization of $1.29\ \mu_B$ per formula unit (f.u.) with the PBE GGA, with a magnetic energy of 0.04 eV/f.u. On a per Ni basis, this is $0.18\ \mu_B$ and 5.7 meV

*singhdj@missouri.edu

TABLE I. Calculated internal structural parameters and atomic moments with the PBE GGA of Y_2Ni_7 at the experimental lattice parameters of $a = 4.947$ Å and $c = 36.25$ Å, space group 166, R$\bar{3}$m with hexagonal coordinates. The nearest 12 neighbors are given as "coord."

Atom	x	y	z	coord.	m(μ_B)
Y1 6c	0	0	0.0504	12 Ni	−0.03
Y2 6c	0	0	0.1472	12 Ni	−0.02
Ni1 18h	0.1671	0.8329	0.4430	7 Ni, 5 Y	0.17
Ni2 9e	1/6	1/3	1/3	8 Ni, 4 Y	0.33
Ni3 6c	0	0	0.2782	9 Ni, 3 Y	0.22
Ni4 6c	0	0	0.3883	9 Ni, 3 Y	0.23
Ni5 3b	0	0	1/2	6 Ni, 6 Y	0.10

∼70 K, i.e., only slightly higher than $T_C = 54$ K. This is indicative of being in the strongly itinerant (Stoner) limit. It is notable that the moment size is ∼0.1 μ_B higher than the reported experimental value. The spin density is illustrated in Fig. 2. The moments on the different Ni sites, as determined by the spin magnetization in the corresponding LAPW spheres, vary considerably as seen in Table I. There is a small back polarization in the interstitial and around the Y atoms, as is commonly found in 3d transition metal ferromagnets. This interstitial spin density is derived from extended orbitals, such as the metal s states. The two Ni sites with low numbers of Ni neighbors (Ni1 and Ni5) have the lowest moments, with Ni5 by far the lowest. However, there is not a clear correlation between coordination and the Ni moment for the other sites.

Calculations for fcc Ni done in the same way yield an ordered moment of 0.635 μ_B and a magnetic energy of 0.062 eV/atom ∼740 K (cf. $T_C = 627$ K). Spin-orbit coupling has only a very small effect, reducing the spin moment by less than 0.01 μ_B/f.u. and producing orbital moments of 0.007 μ_B–0.025 μ_B per Ni, depending on the specific site, always aligned with the spin moment, as expected from the third Hund's rule. The effect of spin orbit coupling on the electronic structure is also very small. This is seen in the band

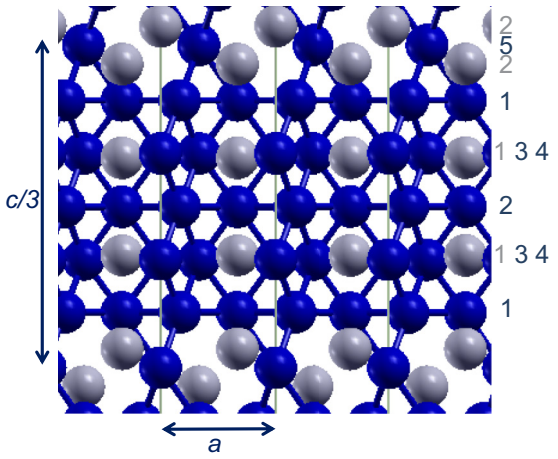

FIG. 1. (Color online) Crystal structure of Y_2Ni_7 showing the layering of the metal atoms. Y is shown as light grey, with Ni as dark blue. The numbers denote the atom number as in Table I.

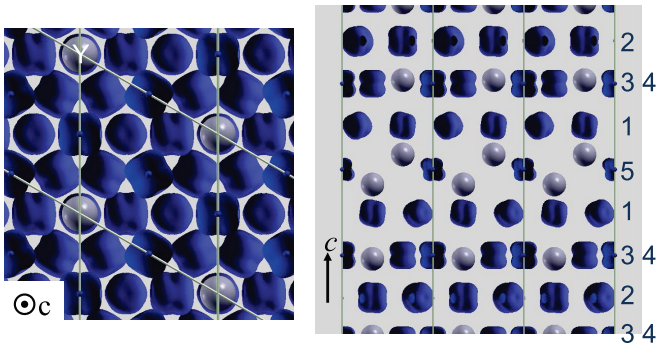

FIG. 2. (Color online) Spin density plot showing the orbital character of the magnetization. The left panel shows a view along the c axis while the right panel is perpendicular to the c axis. The labels indicate the Ni atoms each layer along c, as in Fig. 1. Note the pronounced anisotropy around the Ni atoms.

structure near the Fermi energy E_F, which is given in Fig. 3 in a scalar relativistic approximation and with spin orbit coupling. In the following, we give scalar relativistic results.

With the LSDA, we still obtain an overestimation of the ordered moment, although somewhat smaller, specifically, $M_{\rm LSDA} = 1.17\ \mu_B$/f.u. and $\delta E_{\rm LSDA} = 0.027$ eV/f.u. or ∼47 K on a per Ni basis, i.e., slightly less than T_C. This similarity of the magnetic energy to the experimental T_C is similar to what was found for Ni_3Al [21], suggesting a similarity of Y_2Ni_7 and Ni_3Al. However, it should be noted that the more complicated noncubic structure of Y_2Ni_7 may lead to larger experimental uncertainty in the determination of the moment size due to magnetocrystalline anisotropy and more possibilities for intrinsic defects.

The calculated electronic density of states and projections of Ni d and Y d character are given in Fig. 4, both for the non-spin-polarized and the ferromagnetic cases. As shown, there is a sharp peak in the density of states almost exactly at E_F. The high value leads to a Stoner instability and ferromagnetism, with an exchange splitting of the Ni d bands, although not in a perfect rigid band fashion (note the change in the shape of the exchange split peak between majority and minority spin). Also, the Y d states are above E_F in this compound. In contrast, Y metal is a transition element with ∼2 d electrons. This implies a charge transfer from the Y d states to the Ni host matrix. This is not surprising in view of the electropositive nature of Y relative to Ni. Based on integration of the Ni d density of

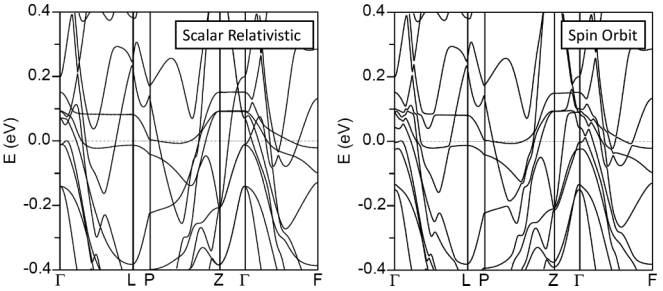

FIG. 3. Band structure of non-spin-polarized Y_2Ni_7 as obtained with the PBE GGA in a scalar relativistic approximation (left) and with spin-orbit coupling (right).

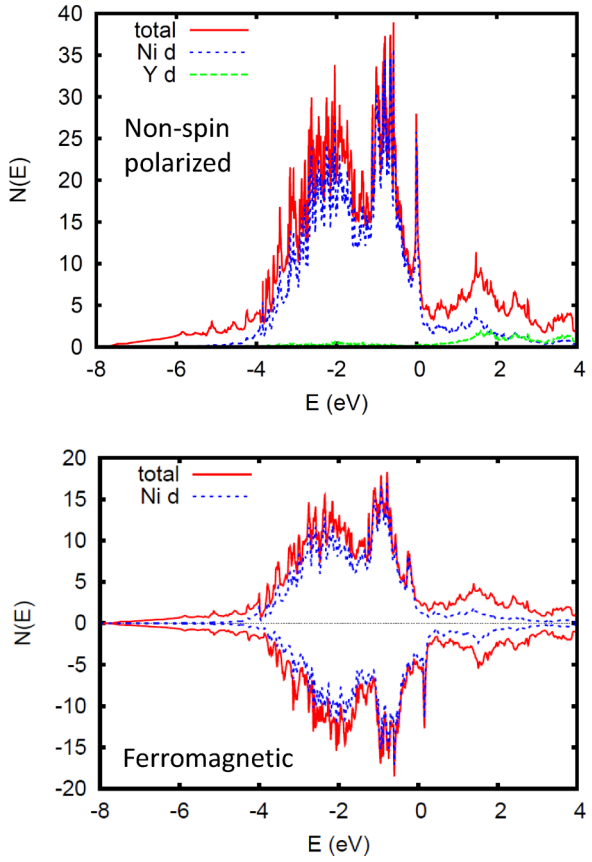

FIG. 4. (Color online) Electronic density of states of Y_2Ni_7 as obtained with the PBE GGA for non-spin-polarized (top) and ferromagnetic (bottom) states.

states in comparison with fcc Ni, most of this charge transfer is to the s electrons. This inference is based on the fact that the d electron count of Ni does not show an increase commensurate with the additional charge.

Within Stoner theory [36,37] the susceptibility of a metal is given by a random phase approximation (RPA) formula, $\chi = \chi_0/[1 - N(E_F)I]$, where χ_0 is the bare Pauli susceptibility, $\chi_0 = \mu_B^2 N(E_F)$, with appropriate units. This formula is exact at the level of band-structure calculations, but neglects the effects of spin fluctuations, which can renormalize the spin susceptibility (see Ref. [38] for a detailed discussion applied to Pd, which is a high susceptibility paramagnetic metal). The Stoner theory itinerant ferromagnetic instability occurs when $N(E_F) = I^{-1}$, which is the point where the RPA enhancement factor $1/[1 - N(E_F)I]$ diverges.

In contrast to standard local moment magnetic materials, in the itinerant limit a metal with properties determined by the non-spin-polarized electronic structure occurs above T_C. There is typically a second-order or near-second-order phase transition at T_C. In Y_2Ni_7, this is a rather interesting metallic state in part because of the high density of states.

We obtain $N(E_F) = 24.0$ eV^{-1} per f.u. on a both spins basis. This well above the criterion for Stoner magnetism, [8,36,37] $N > I^{-1}$ where I is 0.7–0.9 eV for heavy $3d$ transition elements [39] and N is $N(E_F)$ expressed on a per atom per spin basis (1.71 eV^{-1} in the present case). The fixed

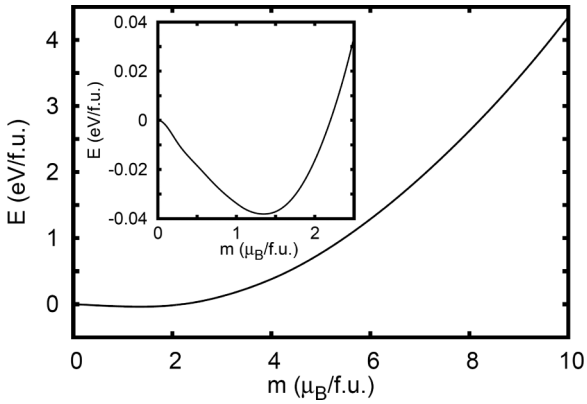

FIG. 5. Fixed spin moment energy as a function of constrained magnetization. The inset shows an expanded scale for low magnetizations.

spin moment energy (Fig. 5) as a function of magnetization therefore drops quickly from zero but then rises because of the narrowness of the peak. The curve is featureless and smooth except for the minimum corresponding to the ferromagnetic ground state. There is no sign of any metamagnetic state at higher magnetization.

The peak at E_F is derived from Ni d orbitals on the Ni2, Ni3, and Ni4 sites, with a somewhat smaller contribution from the Ni1 site and practically no contribution from the Ni5 site. This mirrors the distribution of the moments in the ferromagnetic state. For an atom with trigonal site symmetry (i.e., axial with a three fold axis), as are the Ni3, Ni4, and Ni5 atoms, the d electron crystal field levels are a singly degenerate a_g (z^2, with z along the axis), and two double degenerate e_g levels ($x^2 - y^2$+xy and xz+yz). The Ni3 and Ni4 contributions to the peak at E_F are from the e_g (xz+yz) orbital. The Ni1 and Ni2 contributions are from the same two d orbitals in this reference frame, but not in equal proportion reflecting the lower site symmetry. The orbital character is reflected in the spin density (Fig. 2), where the lobes corresponding to these orbitals are seen around the Ni sites. As seen in the figure, these orbitals are not oriented favorably for bonding interactions, which is a fact consistent with the narrowness of the peak.

The magnetic behavior found in the calculations is consistent with what is expected from extended Stoner theory based on the sharply peaked density of states. Within the extended Stoner theory [40,41], which involves a rigid band approximation, one exchange splits the density of states to obtain magnetization. The stationary solutions are points for which $\overline{N(m)} = I^{-1}$, where $\overline{N(m)}$ is the average density of states between the position of the Fermi level for the minority spin and that for the majority spin to obtain the magnetization m using the non-spin-polarized density of states.

In other words, $\overline{N(m)}$ is the magnetization divided by the energy shift between the majority and the minority spin densities of states needed to produce this magnetization. Thus a sharp peak with little area underneath it will yield a strong initial ferromagnetic instability in a fixed spin moment plot, but will not lead to a high magnetization. This is the origin of the high T_C with low moment. In other words, a narrow peak with a very high $N(E_F)$ leads to a strong initial instability,

i.e., a large negative $\chi = \chi_0/[1 - N(E_F)I]$. However, if the weight under the peak is small, the net magnetization will be low because $\overline{N(m)}$ will not be large for finite m since it is an integral. Note also that the extended Stoner formula uses the connection between the moment size and the exchange splitting through the fact that the moment is an integral of the density of states over the energy range coming from the exchange splitting. This connects the moment, the exchange splitting and the magnetic energy.

The density of states at the Fermi level is reduced to $N(E_F) = 9.1$ eV^{-1} per f.u., mainly from the minority spin in the ferromagnetic ground state. The majority and minority spin contributions are $N_\uparrow(E_F) = 2.8$ eV^{-1} and $N_\downarrow(E_F) = 5.3$ eV^{-1}, respectively. This corresponds to a bare specific heat coefficient, $\gamma_{\rm bare} = 18.9$ mJ/(mol K^2) on a per f.u. basis. It would be interesting to compare with experiment to determine the specific heat enhancement, $\gamma/\gamma_{\rm bare}$, which if large might be an indicator of quantum spin fluctuations.

We now return to the non-spin-polarized case, which should correspond to the electronic structure above T_C in this itinerant material. The band structure (Fig. 3) shows heavy bands close to E_F, specifically the band just below E_F along a large part of the Γ-L line and the band at E_F along P-Z. In addition there are several much more dispersive bands crossing E_F. The consequence is that although the value of $N(E_F)$ is high, the material can have a reasonable conductivity. This multisheet Fermi surface characteristic also occurs in Ni_3Ga and Ni_3Al. [19,21] In general the conductivity can be written as $\sigma \propto \omega_p^2 \tau$, where τ is an effective inverse scattering rate and ω_p is the plasma frequency. We obtain plasma energies $\hbar\omega_p$ of $\Omega_{p,a} = 2.3$ eV and $\Omega_{p,c} = 2.0$ eV, for the basal plane and c-axis directions, respectively. The implied conductivity anisotropy is modest, $\sigma_a/\sigma_c \sim 1.3$. The anisotropy increases in the low temperature ferromagnetic state, for which we obtain $\sigma_a/\sigma_c \sim 1.8$. Also, even though the magnetization is small we obtain a significant transport spin polarization, defined by $P = (\sigma_\uparrow - \sigma_\downarrow)/(\sigma_\uparrow + \sigma_\downarrow)$. We obtain $P = 0.09$ both in the basal plane and c-axis directions.

As mentioned, Y_2N_7 has a remarkably high ordering temperature in relation to its moment. Most magnetic materials are described in terms of local moments and their interactions through the interatomic exhange couplings $J_{i,j}$. These describe spin wave dispersions, which are transverse in character. Longitudinal degrees of freedom, which correspond to changes in the local moment size are hard and not involved in the phase transition. This leads to a simplification in which one can treat the phase transition using the effective spin Hamilitonian and the effect of increasing temperature as the excitation of spin waves. This local moment case has been well described theoretically and numerical simulations of the temperature dependent magnetic properties and phase transitions are practical even for complex systems [42,43]. Importantly, the paramagnetic state above the ordering temperature is a disordered local moment state in which the local moment directions may be regarded as fluctuating in time but retaining their size. This means that the atomic Hund's rule energy associated with the moment formation (i.e., the longitudinal degree of freedom) is not involved in the phase transition as this contribution to the magnetic energy is present in both the ordered and paramagnetic phases.

The itinerant limit has excitation of both transverse and longitudinal degrees of freedom with temperature through coupling to the electronic system and is not describable by an effective spin Hamiltonian. This is more difficult to treat theoretically as it involves coupling to the electrons without separation of electronic and magnetic degrees of freedom. Y_2Ni_7 and Ni_3Al are both apparently close to this limit, and based on comparison of density functional results with experiment both also have renormalizations of their ground states due to quantum fluctuations. Itinerant magnets also have magnetic contributions to the energy in the paramagnetic state [44], above but close to the ordering temperature. However, these are reduced as the moment size is reduced, and in the itinerant limit become negligible. This means that in the itinerant limit all of the magnetic energy including the onsite Hund's energy is available to drive the ordering, providing an explanation for the high ordering temperatures relative to the moments in these itinerant materials. In other words, in itinerant magnets disordering implies destroying the moments, which has an energy cost from the on-site Hund's energy and this leads to high ordering temperatures. We note that the Stoner model of itinerant magnetism has a parallel in the Slater model of itinerant antiferromagnetism and that high ordering temperatures in certain antiferromagnets have been discussed in a way similar to the above [45–47]. In neither case (itinerant or local moment magnets), can energy differences by themselves be simply interpreted as the ordering temperature.

IV. SUMMARY AND CONCLUSIONS

We report density functional calculations of the electronic structure and magnetic properties of Y_2Ni_7. Y_2Ni_7 shows similarity to the weak itinerant ferromagnet Ni_3Al, which has a modest renormalization of the magnetism due to nearness to a quantum critical point. The overestimation of the magnetization relative to experiment is a bit smaller in Y_2Ni_7 implying perhaps somewhat weaker fluctuation effects. This is in contrast to Ni_3Ga, where magnetic ordering is apparently completely suppressed by quantum spin fluctuations. The weak itinerant ferromagnetism in Y_2Ni_7 arises from a Stoner instability of a rather interesting metallic state. This state features a very narrow density of states peak at E_F, a mixture of dispersive and flat bands crossing E_F, and a modest but non-negligible anisotropy of the plasma frequency. Thus Y_2Ni_7 is a uniaxial analog of cubic Ni_3Al. It will be of interest to study the low temperature properties of Y_2Ni_7, its magnetic fluctuations, and the pressure dependence of the magnetic, thermodynamic, and transport properties in comparison with Ni_3Al.

ACKNOWLEDGMENTS

A portion of this work was performed at Oak Ridge National Laboratory with support from the Department of Energy, Basic Energy Sciences, Materials Sciences and Engineering Division.

[1] D. C. Johnston, Adv. Phys. **59**, 803 (2010).
[2] M. D. Lumsden and A. D. Christianson, J. Phys. Condens. Matter **22**, 203203 (2010).
[3] I. I. Mazin, M. D. Johannes, L. Boeri, K. Koepernik, and D. J. Singh, Phys. Rev. B **78**, 085104 (2008).
[4] F. Bondino, E. Magnano, M. Malvestuto, F. Parmigiani, M. A. McGuire, A. S. Sefat, B. C. Sales, R. Jin, D. Mandrus, E. W. Plummer, D. J. Singh, and N. Mannella, Phys. Rev. Lett. **101**, 267001 (2008).
[5] D. J. Scalapino, E. Loh, and J. E. Hirsch, Phys. Rev. B **34**, 8190 (1986).
[6] N. D. Mathur, F. M. Grosche, S. R. Julian, I. R. Walker, D. M. Freye, R. K. W. Haselwimmer, and G. G. Lonzarich, Nature (London) **394**, 39 (1998).
[7] M. D. Johannes, I. I. Mazin, D. J. Singh, and D. A. Papaconstantopoulos, Phys. Rev. Lett. **93**, 097005 (2004).
[8] T. Moriya, Proc. Jpn. Acad. B **82**, 1 (2006).
[9] I. I. Mazin, D. J. Singh, M. D. Johannes, and M. H. Du, Phys. Rev. Lett. **101**, 057003 (2008).
[10] K. Kuroki, S. Onari, R. Arita, H. Usui, Y. Tanaka, H. Kontani, and H. Aoki, Phys. Rev. Lett. **101**, 087004 (2008).
[11] D. J. Scalapino, Rev. Mod. Phys. **84**, 1383 (2012).
[12] N. Buis, J. J. M. Franse, J. Van Haarst, J. P. J. Kaandorp, and T. Weesing, Phys. Lett. A **56**, 115 (1976).
[13] P. G. Niklowitz, F. Beckers, G. G. Lonzarich, G. Knebel, B. Salce, J. Thomasson, N. Bernhoeft, D. Braithwaite, and J. Flouquet, Phys. Rev. B **72**, 024424 (2005).
[14] M. Shimizu, Rep. Prog. Phys. **44**, 329 (1981).
[15] T. Moriya, *Spin Fluctuations in Itinerant Electron Magnetism* (Springer, Berlin, 1985).
[16] F. R. de Boer, C. J. Schinkel, J. Biesterbos, and S. Proost, J. Appl. Phys. **40**, 1049 (1969).
[17] N. R. Bernhoeft, S. M. Hayden, G. G. Lonzarich, D. McK. Paul, and E. J. Lindley, Phys. Rev. Lett. **62**, 657 (1989).
[18] N. R. Bernhoeft, I. Cole, G. G. Lonzarich, and G. L. Squires, J. Appl. Phys. **53**, 8204 (1982).
[19] S. M. Hayden, G. G. Lonzarich, and H. L. Skriver, Phys. Rev. B **33**, 4977 (1986).
[20] H. Winter, Z. Szotek, and W. M. Temerman, Solid State Commun. **74**, 547 (1990).
[21] A. Aguayo, I. I. Mazin, and D. J. Singh, Phys. Rev. Lett. **92**, 147201 (2004).
[22] R. P. Smith, J. Phys. Condens. Matter **21**, 095601 (2009).
[23] A. V. Virkar and A. Raman, J. Less Common Met. **18**, 59 (1969).
[24] K. H. J. Buschow and A. S. Van Der Goot, J. Less Common Met. **22**, 419 (1970).
[25] C. Collinet, A. Pasturel, and K. H. J. Buschow, J. Appl. Phys. **62**, 3712 (1987).
[26] K. H. J. Buschow, J. Less Common Met. **97**, 185 (1984).
[27] R. Lemaire, D. Paccard, and R. Pauthenet, C.R. Acad. Sci. Paris **B264**, 1280 (1967).
[28] J. Inoue, Physica B **149**, 376 (1988).
[29] Y. Nishihara and S. Ogawa, J. Phys. Soc. Jpn. **60**, 300 (1991).
[30] A. Bhattacharyya, D. Jain, V. Ganesan, S. Giri, and S. Majumdar, Phys. Rev. B **84**, 184414 (2011).
[31] R. Z. Levitin, A. S. Markosyan, A. B. Petropavlovskii, and V. V. Snegirev, Phys. Solid State **39**, 1633 (1997).
[32] R. Ballou, B. Gorges, P. Molho, and P. Rouault, J. Magn. Magn. Mater. **84**, L1 (1990).
[33] J. P. Perdew, K. Burke, and M. Ernzerhof, Phys. Rev. Lett. **77**, 3865 (1996).
[34] D. J. Singh and L. Nordstrom, *Planewaves Pseudopotentials and the LAPW Method*, 2nd ed. (Springer, Berlin, 2006).
[35] P. Blaha, K. Schwarz, G. Madsen, D. Kvasnicka, and J. Luitz, WIEN2K, *An Augmented Plane Wave + Local Orbitals Program for Calculating Crystal Properties* (K. Schwarz, Tech. Univ. Wien, Austria, 2001).
[36] E. C. Stoner, Proc. R. Soc. London Ser. A **169**, 339 (1939).
[37] O. Gunnarsson, J. Phys. F **6**, 587 (1976).
[38] P. Larson, I. I. Mazin, and D. J. Singh, Phys. Rev. B **69**, 064429 (2004).
[39] J. F. Janak, Phys. Rev. B **16**, 255 (1977).
[40] O. K. Andersen, J. Madsen, U. K. Poulsen, O. Jepsen, and J. Kollar, Physica B **86–88**, 249 (1977).
[41] G. L. Krasko, Phys. Rev. B **36**, 8565 (1987).
[42] A. I. Liechtenstein, M. I. Katsnelson, and V. A. Gubanov, J. Phys. F **14**, L125 (1984).
[43] K. Sato, W. Schweika, P. H. Dederichs, and H. Katayama-Yoshida, Phys. Rev. B **70**, 201202 (2004).
[44] J. P. Staunton, A. Marmodoro, and A. Ernst, J. Phys. Condens. Matter **26**, 274210 (2014).
[45] E. E. Rodriguez, F. Poineau, A. Llobet, B. J. Kennedy, M. Avdeev, G. J. Thorogood, M. L. Carter, R. Seshadri, D. J. Singh, and A. K. Cheetham, Phys. Rev. Lett. **106**, 067201 (2011).
[46] Y. G. Shi, Y. F. Guo, S. Yu, M. Arai, A. A. Belik, A. Sato, K. Yamaura, E. Takayama-Muromachi, H. F. Tian, H. X. Yang, J. Q. Li, T. Varga, J. F. Mitchell, and S. Okamoto, Phys. Rev. B **80**, 161104 (2009).
[47] D. J. Singh, Phys. Rev. B **91**, 214420 (2015).